Interedge van der Waals interaction between two-dimensional materials

Zepu Kou, Fangyuan Chen, Zonghuiyi Jiang, Wanlin Guo,* and Xiaofei Liu†
State Key Laboratory of Mechanics and Control for Aerospace Structures, Nanjing University of Aeronautics and Astronautics, 210016 Nanjing, China

(Received 15 May 2023; accepted 30 August 2023; published 14 September 2023)

Interedge van der Waals interactions between coplanar two-dimensional metals or semimetals are investigated via the coupled-plasmon approach and many-body dispersion theory. Unlike the "standard" power law $E \sim d^{-3}$ derived from pairwise theory, the nonretarded zero-point energy does not scale with interedge distance as a power law, with the slope of the $\ln(-E)$-$\ln(d)$ relation changing from ~ -1 at 2 Å to ~ -3 at 10 Å. The attractive force for two 10 nm long parallel edges of graphene separated by 4 Å can be up to 6.8 nN, implying that the interedge dispersion force at subnanometer separations might be experimentally detectable. We further show that the interaction can be partly screened by dielectric environments, with the strength of screening being sensitive to whether both surfaces are covered and decaying with the interlayer separation from dielectric substrates.

DOI: 10.1103/PhysRevB.108.115420

I. INTRODUCTION

Two-dimensional (2D) materials with lattices periodically extending in a single plane are the thinnest substances in nature [1,2]. Quantum confinement endows them with novel properties absent in their bulk counterparts, such as the massless fermion of graphene [3], the direct band gap of monolayer molybdenum disulfide [4], great elastic strength and flexibility [5,6], and intrinsically anisotropic optical response [7,8]. Since almost all atoms of a 2D material are on its surface and in direct contact with surrounding environments, the van der Waals (vdW) force [9–11], a fluctuation-induced interaction existing between any charged or neutral substances, is important for interlayer interactions. To name a few, the vdW force is crucial for the ultralow friction between incommensurate layered materials [12], the fabrication of atomically thin crystals via micromechanical cleavage [2], the physisorption of molecules [13], the adhesive strength between 2D interfaces [14–16], and the slippage of water on graphite [17]. For this reason, a lot of efforts have been devoted to the research of interlayer interaction via either density functional theory (DFT) [18,19], *ab initio* random phase approximation [20], or atomic force microscopy (AFM) with naked or wrapped tips [14,21].

On the other hand, the vdW interaction of open edges of finite-size 2D flakes may be as important as the interlayer one. For example, the dispersion interaction participates in the pinning effect between edge and substrate that significantly contributes to the friction of a 2D material [22,23] and dominates the adsorption of free atoms on the growing edge during chemical vapor deposition [24,25]. It may also influence a lot of edge-related properties, such as the ferromagnetic spin order of the graphene zigzag edge [26,27], the plasmon resonance of graphene ribbons tunable with interedge separation [28,29], and the edge stress and stability [30,31]. In spite of the aforementioned importance, the vdW interaction of the edge has seldom been investigated either theoretically or experimentally.

Existing theories of vdW interaction can be categorized into two types. The first type is the atomic-scale theories including density functional theory (DFT)-based vdW approaches and *ab initio* theories [32–36], being perfectly suitable for the interlayer interaction between 2D materials with in-plane periodicity. However, because of the missing of in-plane periodicity along the direction perpendicular to the edge, the interedge vdW interaction between two coplanar semi-infinite 2D monolayers poses a challenge to the atomic-scale theories. The second type is the continuum theories such as the Lifshitz theory or the coupled-plasmon approach (CPA) [37–40], which calculate the zero-point energy of electromagnetic fields or surface plasmons as a function of separation. For parallel semi-infinite half spaces or parallel 2D monolayers, the eigenfrequencies of coupled surface plasmons are usually analytical functions of wave vector and interlayer distance; thus the CPA results in energy-distance relations in the form of simple power laws. Differently, as revealed by Fetter *et al.* [41], Xia and Quinn, [42], and Wang *et al.* [43], the eigenfrequencies of edge plasmons in an open edge of a 2D metal or semimetal cannot be analytically expressed as a function of the wave vector; hence it is unclear whether the CPA would result in a power law for the interedge energy.

In this work, we investigate the interedge vdW interaction between coplanar 2D metallic/semimetallic materials, borophene [44,45], and graphene and silicene [46,47]. By expressing the surficial electrical conductivities with Drude-like models, the interedge energies at a distance ranging from 2 to 10 Å are calculated via the coupled-plasmon approach. It will be shown that the nonretarded interedge energy does not scale with distance as a power law, in stark contrast to the "standard" power law with an exponent of −3 obtained by

*wlguo@nuaa.edu.cn
†liuxiaofei@nuaa.edu.cn

summation of interatomic pairwise energies. The many-body dispersion (MBD) theory leads to a scaling trend similar to that of the CPA, though with relatively faster spatial decay due to finite-width ribbons used for simulation. The attractive forces between 10 nm long parallel edges separated by sub-nanometer distances are evaluated and a possible strategy for experimental detection is discussed. At last, the screening effect of the dielectric environment on the interedge interaction is investigated via both the CPA and the MBD.

II. THEORETICAL METHODS

VdW energy is a manifestation of Coulomb interaction between quantum fluctuation induced spontaneous dipoles. For intersurface or interlayer interactions, the vdW energy can be thought as the zero-point energy of surface plasmons varying with distance because of the distance-dependent Coulomb interaction. For the interedge interaction between two coplanar semi-infinite 2D materials [see illustration in Fig. 1(a)], the vdW energy is just the difference of zero-point energy of coupled edge plasmons relative to that at infinite distance ($d \to \infty$),

$$E_{\mathrm{CPA}} = \frac{1}{2\pi}\int_{-\infty}^{+\infty}\frac{\hbar}{2}[\omega_+(q)+\omega_-(q)-2\omega_e(q)]dq, \qquad (1)$$

where $\hbar$ is the Planck constant, q the one-dimensional wave vector along the edge, ω_+ and ω_- are the two lowest eigenfrequencies of coupled plasmons, and ω_e is the eigenfrequency of an uncoupled edge. Since a short distance range (2–10 Å) is considered here, we ignore the retardation effect due to finite light speed [48,49]; namely, the eigenfrequencies are calculated by solving the electrostatic Poisson equation. For comparison, the interedge vdW energies are also calculated using the pairwise theory and the MBD theory [33].

A. Self-consistent integral equation of electric potential

For simplicity, the metallic borophene and semimetallic graphene and silicene are assumed to be infinitely thin and the surficial electric responses are described by Drude-like local conductivities. The surficial conductivity of borophene [50] is expressed as

$$\sigma(\omega) = \frac{e^2}{m}\frac{i}{\omega + i\tau^{-1}}n, \qquad (2)$$

where e is the electron charge, m is the effective carrier mass, and n is the carrier concentration. The relaxation time τ is discarded in actual calculations. According to the work of Huang *et al.* based on *ab initio* theory [51], n_0 of borophene is 3.4×10^{15} cm^{-2} and m is 3.7 times that of a free electron. For a 2D semimetal with a Dirac cone, the surficial conductivity derived from the band structure reads [52]

$$\sigma(\omega) = \frac{e^2}{\pi^{1/2}\hbar}\frac{v_F}{\omega + i\tau^{-1}}\frac{i}{\sqrt{n}}, \qquad (3)$$

where v_F is the Fermi velocity. For graphene and silicene, v_F are 10^6 and 5.5×10^6 m/s [53,54], respectively. The carrier concentrations of both semimetals are set to a moderate value of 10^{12} cm^{-2} [53,55].

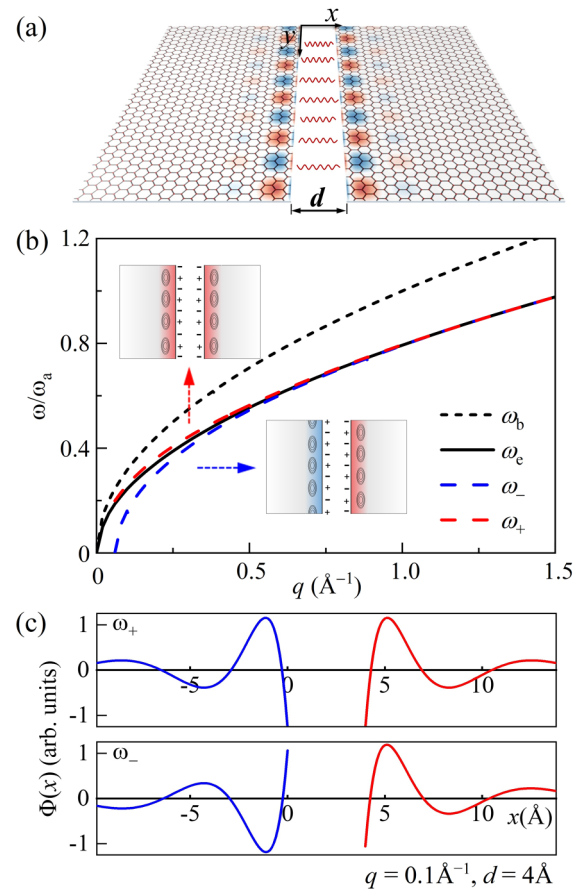

FIG. 1. (a) Schematic illustration of a coupled edge plasmon of two coplanar semi-infinite 2D metallic/semimetallic materials. The color plot represents the spatial distribution of in-plane electric potential. (b) Plasmon frequency as a function of wave vector. ω_b and ω_e denote the plasmon of an intact borophene and an uncoupled borophene edge, respectively. ω_- and ω_+ are the two lowest eigenfrequencies of coupled borophene edges at $d = 4$ Å. The two insets represent the antisymmetric (ω_+) and symmetrical (ω_-) modes, respectively. ω_a is the plasmon frequency of intact 2D borophene at $q = 1/a$. (c) Electric potential profiles of ω_+ and ω_- modes along the x axis, calculated at $q = 0.1$ Å^{-1} and $d = 4$ Å.

Fetter *et al.* [41], Xia and Quinn [42], and Wang *et al.* [43] have investigated the plasmon dispersion relations of uncoupled edges of 2D electron gas and graphene. The numerical method here to calculate the interedge vdW energy is partly inspired by these works. Generally, the plasmon modes of a 2D material can be solved by combining the Poisson equation with the charge conservation law and the constitutive relation between electric field and current. Under an electron density fluctuation $\delta n(\boldsymbol{r})$ within the $z = 0$ plane, the electric field obeys Gauss's law:

$$\nabla \cdot [\varepsilon \boldsymbol{E}(\boldsymbol{r})] = -e\delta n(\boldsymbol{r}). \qquad (4)$$

Here, ε is the background dielectric constant, which is vacuum unless specifically stated. Assuming that $\delta n(\boldsymbol{r})$ is time harmonic, the charge conservation law reads

$$\nabla \cdot \boldsymbol{j}(\boldsymbol{r}) = -ie\omega\delta n(\boldsymbol{r}). \qquad (5)$$

The constitutive equation relating the current density $\boldsymbol{j}$ to the electric field $\boldsymbol{E}$ is

$$\boldsymbol{j}(\boldsymbol{r}) = \sigma(\boldsymbol{r}, \omega) \cdot \boldsymbol{E}(\boldsymbol{r}), \tag{6}$$

where σ becomes position dependent because of the appearance of the edge.

According to Eq. (4) and the fact that $\delta n(\boldsymbol{r})$ is confined in the $z = 0$ plane, the electric potential Φ can be related to the in-plane density fluctuation $\delta n(x, y)$ as

$$\nabla^2 \Phi = \frac{e\delta n(x, y)}{\varepsilon} \delta(z). \tag{7}$$

Thanks to the spatial translational symmetry along the edge (the y axis), the electric potential for an uncoupled edge or two coupled edges can be plane-wave-like, picking up a harmonic factor, $e^{iqy-i\omega t}$. Upon a Fourier transformation in the normal direction (the x axis), Eq. (7) is rewritten as

$$\left[\frac{\partial^2}{\partial^2 z} - (k^2 + q^2)\right] \Phi(k, q, z) = \frac{e\delta n_k}{\varepsilon} \delta(z), \tag{8}$$

where

$$\delta n_k = \frac{1}{2\pi} \int_{-\infty}^{+\infty} e^{-ikx} \delta n(x) dx. \tag{9}$$

Then, the electric potential in the $z = 0$ plane is

$$\Phi(k, q, 0) = -\frac{e\delta n_k}{2\varepsilon (k^2 + q^2)^{1/2}}. \tag{10}$$

By combining Eqs. (5) and (6), the electron density fluctuation can also be related to the electric potential as

$$\delta n(x') = -\frac{1}{ie\omega}\left[-\sigma\left(q^2 - \frac{d^2}{dx'^2}\right)\Phi(x', q, 0) - \frac{d\sigma}{dx'}\frac{d\Phi(x', q, 0)}{dx'}\right]. \tag{11}$$

Finally, a self-consistent integral equation of the electric potential is derived from Eqs. (10) and (11):

$$\Phi(x, q, 0) = \frac{1}{i\omega\varepsilon} \int_{-\infty}^{+\infty} dx' L_q(x - x') \times \left[\sigma\left(q^2 - \frac{d^2}{dx^2}\right) - \frac{d\sigma}{dx'}\frac{d}{dx'}\right]\Phi(x', q, 0). \tag{12}$$

Here, the integration kernel $L_q(x - x')$ is given as

$$L_q(x - x') = \int_{-\infty}^{+\infty} \frac{dk}{4\pi} \frac{e^{ik(x-x')}}{(k^2 + q^2)^{1/2}} = \frac{K_0(q|x - x'|)}{2\pi}, \tag{13}$$

where $K_0(x)$ is a particular Bessel function according to formula 9.6.21 of the *Handbook of Mathematical Functions* [56].

To describe the boundary condition upon the appearance of the edge, $n(r)$ is expressed by the product of n_0 and a boundary-related function $f(x)$. For an uncoupled semi-infinite 2D material in the left half plane, the function is

$$f(x) = \begin{cases} 0, & 0 < x \\ -x/a, & -a < x < 0 \\ 1, & x < -a \end{cases}, \tag{14}$$

where a is the edge width [42]; it is set to a small value of 0.1 Å to avoid having an artificial effect on the energy-distance relation in the short range. For two semi-infinite 2D materials residing in the left and right half planes, respectively, we have

$$f(x) = \begin{cases} -x/a, & -a < x < 0 \\ 0, & 0 < x < d \\ (x - d)/a, & d < x < d + a \\ 1, & x < -a || x > d + a \end{cases}, \tag{15}$$

where d is the interedge distance as illustrated in Fig. 1(a).

By incorporating $f(x)$ into the integral equation, we arrive at the final equation directly used for numerical calculation. For a 2D metal, the integral equation is

$$\Phi(x, q, 0) = \frac{2\omega_a^2}{\omega^2} \int_{-\infty}^{+\infty} dx' L_q(x - x') \times \left[f(x')\left(q^2 - \frac{d^2}{dx^2}\right) - \frac{df(x')}{dx'}\frac{d}{dx'}\right]\Phi(x', q, 0), \tag{16}$$

where $\omega_a = e^2\, n_0/2m\varepsilon a$ is the plasmon frequency of the intact 2D metal at a wave vector of $q = 1/a$. For a 2D semimetal, the integral equation is

$$\Phi(x, q, z = 0) = \frac{2\omega_a^2}{\omega^2} \int_{-\infty}^{+\infty} dx' L_q(x - x') \times \left[\sqrt{f(x')}\left(q^2 - \frac{d^2}{dx^2}\right) - \frac{d\sqrt{f(x')}}{dx'}\frac{d}{dx'}\right]\Phi(x', q, 0), \tag{17}$$

where $\omega_a = e^2\, v_F \sqrt{n_0}/2\sqrt{\pi}\hbar\varepsilon a$ is the plasmon frequency of the intact 2D semimetal at $q = 1/a$.

B. Numerical solution of the integral equation

To solve the self-consistent integral equations, the electric potential can be expanded in Laguerre polynomials [41–43,56]. For an uncoupled edge, the electric potential is expanded as

$$\Phi(x, q, 0) = e^{qx} \sum c_n L_n(-2qx). \tag{18}$$

Then the self-consistent integral equation is transformed to a matrix equation

$$\boldsymbol{Gc} = \frac{\omega^2}{4\omega_a^2 q}\boldsymbol{c}, \tag{19}$$

where $\{c_j\}$ is a set of expansion coefficients; the matrix elements $\{G_{ij}\}$ can be calculated from Eq. (16) or (17). The eigenfrequencies of the edge plasmon can be calculated from the eigenvalues of the matrix equation.

For two coupled edges, the electric potential is expanded with two sets of Laguerre polynomials,

$$\Phi(x, q, 0) = \begin{cases} e^{qx} \sum_{n=0}^{\infty} c_n^1 L_n(-2qx), & x < 0 \\ e^{-q(x-d)} \sum_{n=0}^{\infty} c_n^2 L_n[2q(x - d)], & x > d \end{cases}, \tag{20}$$

where c_n^1 and c_n^2 are the expansion coefficients for the potential on the left and right sides, respectively. The eigenfrequencies of the coupled edge plasmons can be obtained by solving the matrix equation,

$$\begin{bmatrix} \boldsymbol{G}^{11} & \boldsymbol{G}^{12} \\ \boldsymbol{G}^{21} & \boldsymbol{G}^{22} \end{bmatrix} \begin{bmatrix} \boldsymbol{c}^1 \\ \boldsymbol{c}^2 \end{bmatrix} = \frac{\omega^2}{4\omega_a^2 q} \begin{bmatrix} \boldsymbol{c}^1 \\ \boldsymbol{c}^2 \end{bmatrix}, \tag{21}$$

where the submatrices $\boldsymbol{G}^{12}$ and $\boldsymbol{G}^{21}$ originate from the Coulomb interaction between the charge fluctuations on the two sides. In order to ensure accuracy and efficiency, we use a basis set with 20 Laguerre polynomials for each edge. Figure 5 of Appendix A verifies that increasing the basis size from 20 to 30 or 40 does not alter the frequency difference between coupled and uncoupled plasmons, $\omega_+ + \omega_- - 2\omega_e$. We note that the CPA formulation could also work for 2D semiconductors, by replacing Eqs. (5) and (6) with the constitutive relations of surficial dielectric response,

$$\delta n = -\nabla \cdot \boldsymbol{P}_{2\mathrm{D}}, \tag{22}$$

$$\boldsymbol{P}_{2\mathrm{D}} = -\alpha_{2\mathrm{D}} \nabla \Phi(z=0), \tag{23}$$

where $\alpha_{2\mathrm{D}}$ is the 2D polarizability and $P_{2\mathrm{D}}$ is the surficial polarization. Nevertheless, the interedge vdW energy should be given by the adiabatic connection fluctuation-dissipation theorem (ACFDT) instead (see Appendix B for the detailed derivations).

C. Computational details of the pairwise theory and the MBD theory

According to the pairwise theory widely used in the physical chemistry community, the interedge vdW energy can be expressed as the sum of interatomic energies,

$$E_{\mathrm{pairwise}} = \sum -C_6 R_{ij}^{-6}, \tag{24}$$

where the i and j indices denote the atoms on the left and right sides, respectively. For graphene and silicene [15], C_6 coefficients derived from 2D materials' dielectric functions are applied, which are 17.63 and 222.1 hartree bohr^6, respectively. On the other hand, a free-atom C_6 coefficient is used for borophene (99.5 hartree bohr^6) [57], since the 2D Clausius-Mossotti relation [15] for the complex borophene structure is unavailable. For a fair comparison between different theories, the damping function as often used in the DFT-based vdW approach is not included here. The detailed molecular structures and manners of edge alignment are displayed in Fig. 7 of Appendix C. In actual calculations with the pairwise theory, two coplanar ribbons with a width of $\sim$1000 Å are used.

The DFTMBD theory developed by Tkatchenko *et al.* [33] is applied to calculate the interedge vdW energy of graphene. This method considers each atom as a quantum harmonic oscillator and obtains the vdW energy as the difference of zero-point energy of the coupled oscillators relative to that of the isolated ones. Technically, the DFT-MBD calculations are performed using the FHI-AIMS code [58]. A tight basis is used for the orbital and the Perdew-Burke- Ernzerhof functional [59] is applied for the exchange-correlation energy. Due to the limitation of computational cost, the supercell consists of two parallel coplanar armchair ribbons, each with two hexatomic rings along the width direction. To avoid any spurious interactions between periodic images, the height and length of the supercell are set to 20 and 40 Å, respectively. A k-point mesh of $3 \times 1 \times 1$ is used for the momentum space sampling. Notably, the quantum Drude oscillator applied in the MBD theory cannot tackle the vdW energy originating from electrical conduction, which is important in long ranges.

III. RESULTS AND DISCUSSION

A. Uncoupled and coupled edge plasmons

We first look into the dispersion relations of the uncoupled and coupled edge plasmons. As illustrated by the dashed curve in Fig. 1(b), the plasmon frequency of an intact borophene scales with the wave vector as $\omega_{\mathrm{b}} \propto q^{1/2}$, which is a common characteristic of 2D metal. Upon the introduction of the edge, the lowest eigenfrequency is shifted downwards. Because the electric potential fluctuation is mainly localized at the edge and decays in regions far from the edge, this plasmon mode can be attributed to the edge. As we here adopt a rather small edge width $a = 0.1$ Å, the dispersion relation looks akin to that of an abrupt edge [42], $\omega_e \sim (2/3)^{1/2}\omega_b$. In the case of coupled edges, the dispersion curve is split into two different ones: one with higher frequency denoted as ω_+ and another with lower frequency denoted as ω_-. The splitting vanishes with increasing wave vector (at q of $\sim$0.75 Å^{-1} in the case of $d = 4$ Å), which is understandable since the electric potential oscillates periodically along the edge direction [Fig. 1(a)]. Figure 1(c) shows that the amplitudes of the electric potentials of the ω_+ and ω_- modes are symmetric and antisymmetric along the normal direction, respectively. Then ω_+ and ω_- can be defined as the antisymmetric and symmetric modes, because the values of the electric fields of ω_+ and ω_- are antisymmetric and symmetric, respectively. At the absolute zero of temperature, the two lowest modes of the coupled edges will be excited owing to quantum fluctuation, whereas there are two uncoupled edge modes in the $d \to \infty$ case. In the considered range of wave vector, the sum of ω_+ and ω_- is always lower than two times ω_e, resulting in an attractive vdW force.

For completeness, Fig. 6 of Appendix C shows the dispersion relations of edge plasmons calculated with a larger edge width, $a = 1$ Å. The uncoupled edge is seen to support more higher-frequency modes, which are usually termed dipole, quadrupole modes, etc. [42,43]. Here, within the wave vector range shown in Fig. 6, only the dipole mode appears. These modes actually coincide with the 2D bulk mode at small wave vectors, and thus cannot be thought of as pure edge modes. Indeed, due to the larger separation between the charge fluctuations on the two sides, the higher-frequency modes of two coupled edges do not show evident splitting. Since the dipole mode does not appear in the considered wave vector range at $a = 0.1$ Å, we do not consider the effect of higher-frequency modes on the vdW interaction.

The dispersion relation of graphene or silicene edges with a small edge width of $a = 0.1$ Å looks quite akin to those of borophene edges except for the different ω_a; thus to avoid repetition the details are not presented here. The similar dispersion relations of the 2D metal and 2D semimetals are to be expected, if one notices that the integral equations (16) and (17) only differ with each other in the region of edge width.

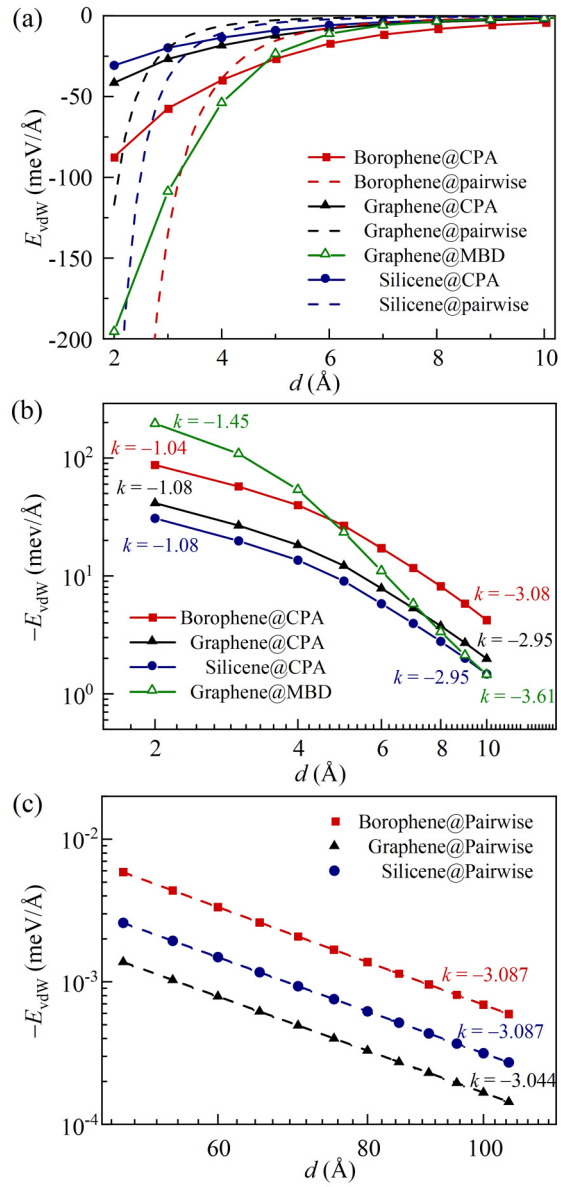

FIG. 2. (a) Interedge vdW energy density between coplanar semi-infinite 2D materials as a function of distance, calculated using the CPA, the pairwise theory, and the MBD (for graphene only). (b) Log-log plot of interedge vdW energy density as a function of separation. The slopes at $d = 2$ and 10 Å are labeled in the figure. (c) Log-log plot of interedge pairwise energy density as a function of separation. To avoid the influence of detailed edge structures, the energies in a medium distance range (50–100 Å) are used for the linear fitting.

B. Interedge vdW energy

Figure 2(a) presents the interedge vdW energy densities E_{vdW} in the distance range from 2 to 10 Å. According to either the CPA or the pairwise theory, the vdW interaction between borophene edges is the strongest among the considered materials. The relatively stronger interaction of borophene predicted by the CPA originates from its larger carrier concentration that is three orders of magnitude higher than those of graphene and silicene, while that predicted by the pairwise theory is mainly due to the relatively larger atomic density of borophene. Among graphene and silicene with the same carrier concentration, the former with higher Fermi velocity exhibits relatively stronger vdW interaction.

We also show the MBD energy of two coplanar narrow graphene ribbons in Fig. 2(a). In the considered distance range, the MBD energy is higher than the CPA energy and the pairwise energy. We note that the MBD energy of graphene edges should be considered as the suitable theoretical value to be compared with the experimental result. The CPA energy of graphene here is underestimated, since the contribution of the dielectric response is not included and only a moderate carrier concentration of graphene is assumed. The pairwise energies here could also be underestimated, in contrast to previous works where the MBD energies tend to be lower than the pairwise ones calculated with free-atom C_6 coefficients. The different relative magnitudes here are due to the fact that the C_6 coefficient derived from the Clausius-Mossotti relation for intact graphene is applied, overestimating the dipole-dipole screening near the edge.

A particular interest of vdW energy is its scaling law as a function of separation. For highly symmetric configurations, the energy-distance relation often obeys a power law with a dimensionality-dependent exponent. For two parallel semi-infinite objects, the dispersion energy scales with distance as $E = -d^{-2}$ [48], while for interlayer energy between 2D monolayers Dobson *et al.* [39] find that the power-law exponent can be -4, -2.5, or -3 depending on whether the materials are metallic, semimetallic, or insulating. In order to reveal the scaling law of interedge energy, the log-log plots of $-E_{vdW}$-d relations calculated from the CPA and the pairwise theory are shown in Figs. 2(b) and 2(c), respectively. The pairwise theory results in a "standard" power law with an exponent of -3, implying that the standard interedge energy has a slower spatial decay than the standard interlayer energy with an exponent of -4 [39]. Previous studies of interlayer energy find that the CPA energy decays with distance more slowly than the pairwise energy does. This is also true for the interedge energy here. However, in sharp contrast to the interlayer case, the interedge CPA energy no longer follows a power law, with the slope of the $\ln(-E)$-$\ln(d)$ relation changing from ~ -1 at 2 Å to ~ -3 at 10 Å. The irregular scaling law should be caused by the reduced symmetry in the configuration of coplanar semi-infinite monolayers. Surprisingly, the MBD results in a scaling trend similar to that by the CPA, though with the slope of the $\ln(-E)$-$\ln(d)$ relation changing from -1.45 to -3.61 in the considered distance range. The faster spatial decay by the MBD is just due to the narrow graphene ribbons used in the DFTMBD calculation. If wider graphene ribbons were used, the scaling trend of the MBD energy should achieve even better agreement with the CPA.

To figure out whether the interedge vdW force could be experimentally detectable, Fig. 3 shows the attractive forces between two 10 nm long flakes. According to the MBD, the interedge force between the graphene flakes can be up to 6.8 nN at $d = 4$ Å. Although this force can be one order of magnitude smaller than that for two parallel 10 nm × 10 nm flakes at an interlayer distance of 4 Å, it is orders of magnitude larger than the detection accuracy of AFM [14]. According to the work of Gao and Tkatchenko [60], the frictional force of a

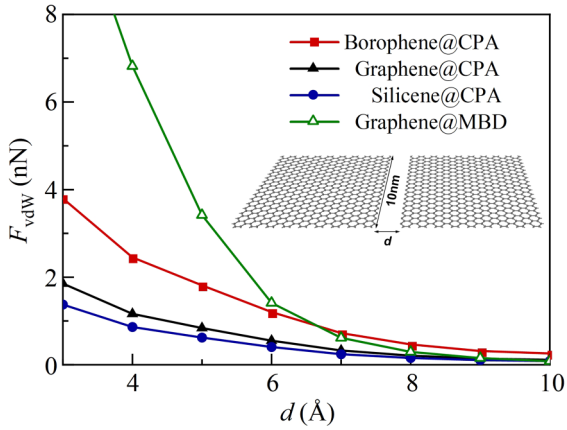

FIG. 3. Interedge vdW force between two 10 nm long flakes as a function of distance.

triangular graphene flake with a side length of 10 nm sliding on another graphene substrate can be down to 3.2 nN. Hence, the interedge force is comparable to the interlayer friction and in some circumstances could overcome the friction and drive the nanoflake. The CPA leads to relatively lower but still sizable vdW forces, which are 2.5, 1.2, and 0.9 nN for borophene, graphene, and silicene at $d = 4$ Å, respectively. Based on the above analyses, we suggest that the experimentalists could measure the interedge force by placing a triangular graphene nanoflake in close proximity to the open edge of another graphene monolayer.

C. Dielectric screening effect on interedge vdW energy

Recent experimental [61] and theoretical works [62–64] demonstrate a so-called vdW screening or Faraday cage–like screening effect; namely, a graphenelike monolayer can partly screen the vdW interaction between objects on its two sides. Actually, this kind of dielectric screening can also influence the interedge vdW interaction, when the two coplanar semi-infinite monolayers are supported or sandwiched by dielectric substrates. Here, we consider the screening effect induced by an ultraflat *h*-BN substrate, an extensively used dielectric substrate for 2D devices [65,66]. To consider the screening effect upon sandwiching the semi-infinite monolayers with thick *h*-BN layers [see illustration in Fig. 4(a)], the background dielectric constant ε in the CPA formulation is replaced with the frequency-dependent dielectric function of $h-$BN expressed by a Lorentz model (see Appendix D). Figure 4(b) shows the vdW energy upon screening, E'_{CPA}, normalized with respect to that without screening, E_{CPA}. With increasing interedge distance, the ratios $E'_{\mathrm{CPA}}/E_{\mathrm{CPA}}$ converge to constant

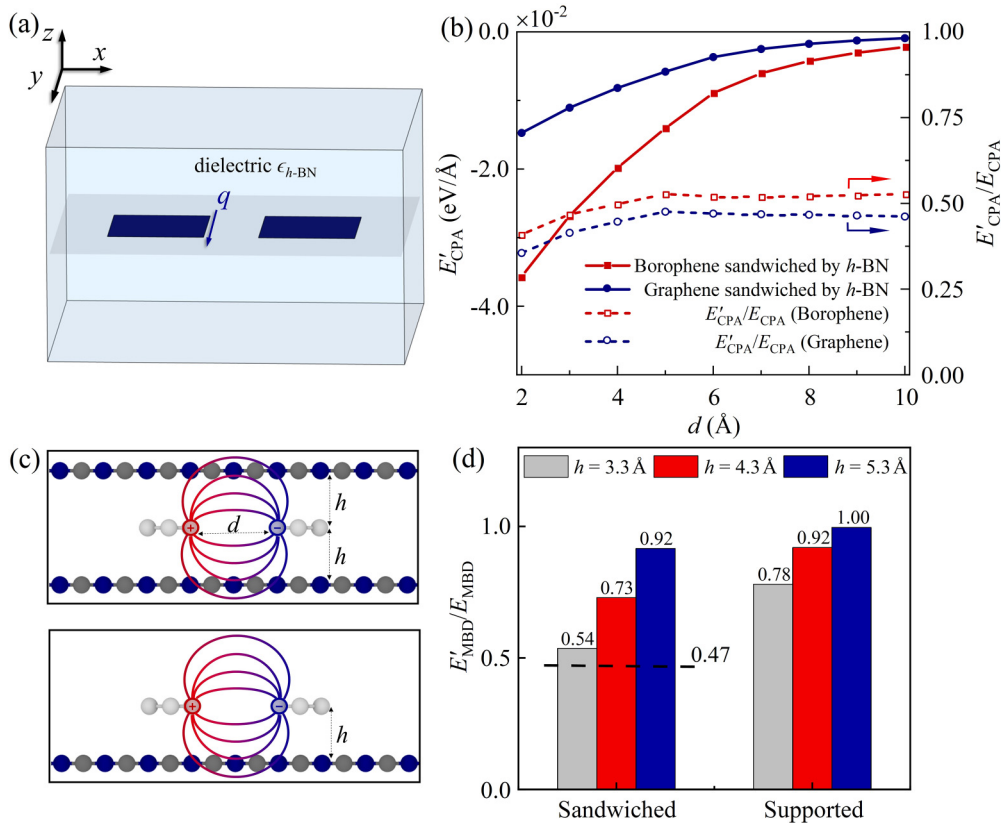

FIG. 4. Dielectric screening effect of *h*-BN substrates on the interedge vdW energy. (a) Schematic illustration of interacting edges sandwiched by bulk *h*-BN. (b) Interedge vdW energy densities for borophene or graphene sandwiched by *h*-BN, calculated using the CPA. (c) Atomic structures of coplanar graphene ribbons sandwiched or supported by monolayer *h*-BN used for the DFTMBD calculations. (d) Ratio of interedge vdW energy of graphene under screening to that without screening, calculated using the DFTMBD. The dashed line denotes the ratio given by the CPA.

values, which are 0.52 and 0.47 for borophene and graphene, respectively, implying that sandwiching the monolayers with *h*-BN substrates can screen off about half the interedge vdW energy.

The vdW screening effect is also investigated via the MBD, which has been shown to be effective for the interlayer vdW screening at short interlayer distances [62,64]. Due to the limitation of computational resources, two coplanar armchair graphene ribbons with one carbon hexagon in the width direction and sandwiched by *h*-BN monolayers are used for the DFTMBD calculations [see Fig. 4(c)]. To avoid the influence of periodic images, the height and length of the supercell are set to 40 and 40 Å, respectively. The interedge MBD energy is calculated as the difference of the MBD energy at $d = 5.025$ Å relative to that at the reference point ($d = 10.050$ Å), because at the two distances the vdW energies between the graphene ribbons and *h*-BN monolayers can remain identical. Surprisingly, at an interlayer distance h of 3.3 Å, the ratio $E'_{\mathrm{MBD}}/E_{\mathrm{MBD}}$ is 0.54 [see Fig. 4(d)], being rather close to the ratio $E'_{\mathrm{CPA}}/E_{\mathrm{CPA}}$ (0.47). We note that the excellent agreements on the screening effect as well as on the scaling trend of interedge energy by the CPA and MBD are rooted in the fact that both theories derive the vdW energy via coupled electromagnetic oscillators, either continuum or atomic ones.

We also investigate the screening effect by merely an underlying *h*-BN monolayer. The ratio $E'_{\mathrm{MBD}}/E_{\mathrm{MBD}}$ at an interlayer distance of 3.3 Å is 0.78, meaning that the strength of the vdW screening effect is less significant when only one side is covered by the dielectric. This can be readily rationalized if one notices that only part of the electric field lines joining the electron and hole passes through the underlying *h*-BN monolayer [Fig. 4(c)]. Figure 4(d) also shows the screening effect as a function of the interlayer separation. As h increases to 5.3 Å, the ratios $E'_{\mathrm{MBD}}/E_{\mathrm{MBD}}$ for the sandwiched and supported edges gradually increase to 0.92 and 1.00, respectively, in good agreement with our anticipation that larger separation will induce weaker screening. We note that this interlayer distance dependence of screening strength is also expected for the interlayer screening, but has not been reproduced by the MBD, at least in the medium range [64].

IV. CONCLUSION

We have studied the interedge nonretarded dispersion interaction between two coplanar semi-infinite 2D metal/semimetals, using the coupled-plasmon approach and the many-body dispersion theory. Due to the reduced symmetry, the interedge energy in the short range (2–10 Å) does not scale with distance as a power law. Compared with the "standard" power law by the pairwise theory, the theories based on the coupled oscillators give slower spatial decay. At subnanometer distances, the interedge attractive forces are sizable and even comparable to the friction of a nanoflake on a flat substrate, and thus could be experimentally detectable. Finally, it is shown that the interedge van der Waals interaction can be partly screened by dielectric substrates, just like the previously revealed dielectric screening effect on the interlayer interaction.

ACKNOWLEDGMENTS

X.L. is supported by the National Natural Science Foundation of China (Grants No. 12072152 and No. 11702132). W.G. is supported by the National Key Research and Development Program of China (Grant No. 2019YFA0705400), and the Fundamental Research Funds for the Central Universities (Grants No. NJ2020003 and No. NZ2020001).

APPENDIX A: CONVERGENCE TEST AND EFFECT OF EDGE WIDTH

Figure 5 shows the frequency differences between the coupled and uncoupled plasmons, $\omega_+ + \omega_- - 2\omega_e$, calculated with bases consisting of 20, 30, and 40 Laguerre polynomials. Increasing the basis size from 20 to 30 or 40 does not lead to obvious improvement on the results, verifying that the basis of 20 Laguerre polynomials is sufficient for the convergence of eigenfrequencies of edge plasmons and interedge energy.

Figure 6 shows the plasmon dispersion of the borophene edge as a function of wave vector q, calculated with an edge width of $a = 1$ Å. In the considered wave vector range (<1.5 Å^{-1}), the larger edge width results in a deviation of the dipole mode from the bulk mode. For two coupled edges, the symmetric and antisymmetric dipole modes coincide with the uncoupled one, which means that the higher-energy modes do not contribute to the interedge vdW energy.

APPENDIX B: ACFDT FORMULATION FOR INTEREDGE vdW ENERGY OF NONMETALLIC 2D MATERIALS

The charge fluctuations of nonmetallic 2D materials comes from the polarization of bound charges of atoms:

$$n_{\mathrm{ind}}(x, y, z = 0) = -\nabla \cdot \boldsymbol{P}_{2\mathrm{D}}(x, y, z = 0). \tag{B1}$$

Here, $\boldsymbol{P}_{2D}$ is the surficial polarization induced by the electric field,

$$\boldsymbol{P}_{2\mathrm{D}}(x, y, z = 0) = -\alpha_{2\mathrm{D}} \nabla \Phi(x, y, z = 0), \tag{B2}$$

with $\alpha_{2\mathrm{D}}$ being the 2D polarizability in the in-plane direction. As the dispersion relation of the plasmon in the semi-infinite

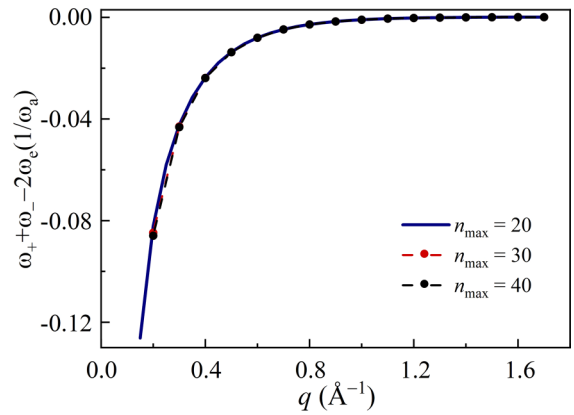

FIG. 5. $\omega_+ + \omega_- - 2\omega_e$ as a function of q, calculated with bases consisting of 20, 30, and 40 Laguerre polynomials.

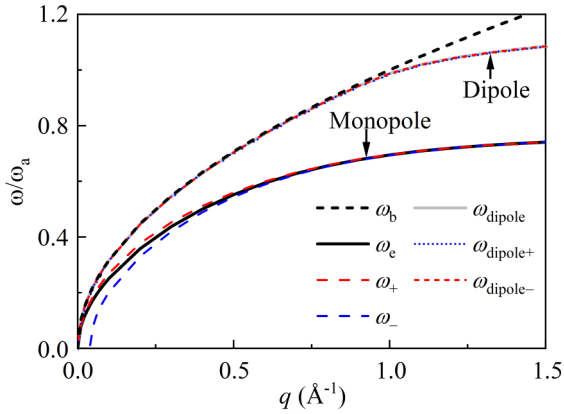

FIG. 6. Plasmon frequency of borophene edge as a function of wave vector, calculated at an edge width of $a = 1$ Å. ω_- and ω_+ are the two lowest eigenfrequencies of coupled modes at $d = 4$ Å. ω_{dipole}, $\omega_{\text{dipole}+}$, and $\omega_{\text{dipole}-}$ are the uncoupled and coupled dipole modes of edge plasmons, respectively.

nonmetallic 2D layers cannot be explicitly derived, the summation of zero-point energies cannot be used to evaluate the interedge vdW energy. Instead, the adiabatic connection fluctuation dissipation theorem (ACFDT) is generally applicable [39], if only the electron density–density response function χ can be explicitly given. The correlation energy reads

$$E_{\text{vdW}} = -\frac{\hbar}{2\pi}\int_0^1 d\lambda \int d\boldsymbol{r}d\boldsymbol{r}'\frac{e^2}{|\boldsymbol{r}-\boldsymbol{r}'|} \times \int_0^\infty \chi_\lambda(\boldsymbol{r},\boldsymbol{r}',iu) - \chi_0(\boldsymbol{r},\boldsymbol{r}',iu)du, \tag{B3}$$

where χ_λ is the charge density response function at the Coulomb interaction scaled by λ and χ_0 is the bare response function. Both χ_λ and χ_0 are functions of the imaginary frequency iu.

Combining Eqs. (B1) and (B2), one obtains the induced charge density under an external potential,

$$n_{\text{ind}}(x,q,0) = \alpha_{2\text{D}}\left[f(x)\left(\frac{d^2}{dx^2}-q^2\right)+\frac{df(x)}{dx}\frac{d}{dx}\right]\Phi(x,q,0), \tag{B4}$$

where the total potential is

$$\Phi(x,q,0) = \Phi_{\text{ext}}(x,q,0) + 2\int_{-\infty}^{+\infty}\lambda K_0[q(|x-x'|)] \times n_{\text{ind}}(x',q,0)dx'. \tag{B5}$$

By linearly expanding the induced charge density n_{ind} and the external potential $\Phi_{\text{ext}}(\boldsymbol{r})$ with the Laguerre polynomials,

$$n_{\text{ind}}(x,q,0) = \begin{cases}\sum_{n=0}^\infty c_n^1\, e^{qx}L_n(-2qx), & x<0\\ \sum_{n=0}^\infty c_n^2\, e^{-q(x-d)}L_n[2q(x-d)], & x>d\end{cases}, \tag{B6}$$

$$\Phi_{\text{ext}}(x,q,0) = \begin{cases}\sum_{n=0}^\infty b_n^1\, e^{qx}L_n(-2qx), & x<0\\ \sum_{n=0}^\infty b_n^2\, e^{-q(x-d)}L_n[2q(x-d)], & x>d\end{cases}, \tag{B7}$$

the charge density response can be described via the linear relation of coefficients of linear expansions,

$$\begin{bmatrix}\boldsymbol{c}^1\\ \boldsymbol{c}^2\end{bmatrix} = \begin{bmatrix}\boldsymbol{R}_{11} & \boldsymbol{R}_{12}\\ \boldsymbol{R}_{21} & \boldsymbol{R}_{22}\end{bmatrix}\begin{bmatrix}\boldsymbol{b}^1\\ \boldsymbol{b}^2\end{bmatrix}, \tag{B8}$$

where $\boldsymbol{R}$ is the response matrix. By left multiplying Eq. (B5) by any basis function and integrating, one obtains a matrix equation of $\boldsymbol{R}$,

$$\frac{1}{2q}\boldsymbol{R} = \boldsymbol{R}_0 + \boldsymbol{A}\boldsymbol{R}, \tag{B9}$$

where $\boldsymbol{R_0}$ is the bare response matrix. The vdW energy per unit length then is

$$E_{\text{vdW}}/L = -\frac{\hbar}{\pi}\int_0^1 d\lambda\int_0^\infty du\int dxdx'\int_0^{-\infty}dq\frac{2\pi}{(2\pi)^2} \times K_0(q|x-x'|)\cdot[\boldsymbol{l}(x')^T(\boldsymbol{R}-\boldsymbol{R}_0)\boldsymbol{l}(x)], \tag{B10}$$

where the elements of vector $\boldsymbol{l}$ are the Laguerre basis functions as applied in Eq. (B6) or (B7).

APPENDIX C: DETAILS OF PAIRWISE THEORY

Figure 7 shows the atomic structures used for the calculations of pairwise vdW energies. To mimic semi-infinite monolayers, the ribbon width is set to be 1000 Å, much larger than the interedge distances. The atomic structures periodically extend along the edge direction. We note that while the crystal structure of the adopted borophene is anisotropic, the optical anisotropy along the x and y axes is insignificant [51] and neglected in this work.

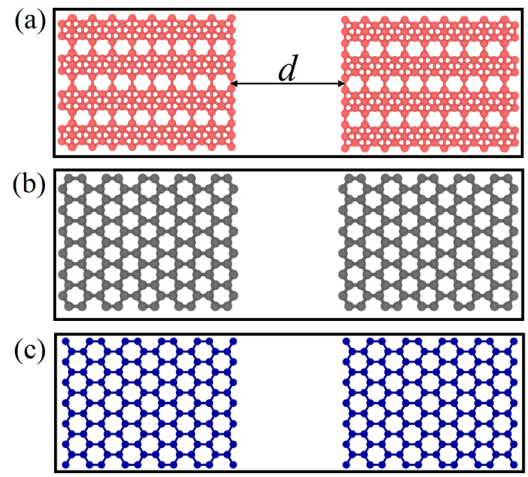

FIG. 7. Atomic structures used for calculations of pairwise vdW energies between (a) borophene, (b) graphene, and (c) silicene edges.

APPENDIX D: DIELECTRIC FUNCTION OF *h*-BN AND EDGE PLASMONS UNDER SCREENING

To calculate the interedge energy under screening, the background dielectric constant ε in the CPA formulation is replaced with the frequency-dependent dielectric function of *h*-BN, which can be expressed by a Lorentz model [67]:

$$\varepsilon_L = \varepsilon_\infty \frac{\omega^2 - \omega_{\mathrm{LO}}^2 + i\gamma\omega}{\omega^2 - \omega_{\mathrm{TO}}^2 + i\gamma\omega}. \tag{D1}$$

Here, ω_{LO} and ω_{TO} are longitudinal optical phonon frequency and transverse optical phonon frequency, respectively; γ is the damping factor; ε_∞ is the high-frequency dielectric constant. Inserting (D1) into Eqs. (19) and (21), we get new matrix equations for the uncoupled and coupled edges, respectively,

$$\boldsymbol{G}\boldsymbol{c} = \frac{\omega^2}{4\omega_a'^2 q}\boldsymbol{c}, \tag{D2}$$

$$\begin{bmatrix} \boldsymbol{G}^{11} & \boldsymbol{G}^{12} \\ \boldsymbol{G}^{21} & \boldsymbol{G}^{22} \end{bmatrix} \begin{bmatrix} \boldsymbol{c}_i^1 \\ \boldsymbol{c}_k^2 \end{bmatrix} = \frac{\omega^2}{4\omega'^2_a q} \begin{bmatrix} \boldsymbol{c}_i^1 \\ \boldsymbol{c}_k^2 \end{bmatrix}, \tag{D3}$$

where ω'_a is the plasmon frequency at a wave vector of $q = 1/a$ for the intact 2D material under screening

$$\omega'^2_a = \frac{\left(\omega^2 + \omega_{\mathrm{TO}}^2 + \gamma\omega\right)\varepsilon_\infty}{\omega_a^2\left(\omega^2 + \omega_{\mathrm{LO}}^2 + \gamma\omega\right)}. \tag{D4}$$

[1] K. S. Novoselov, A. K. Geim, S. V. Morozov, D. Jiang, M. I. Katsnelson, I. V. Grigorieva, S. V. Dubonos, and A. A. Firsov, Two-dimensional gas of massless Dirac fermions in graphene, Nature (London) **438**, 197 (2005).

[2] K. S. Novoselov, D. Jiang, F. Schedin, T. J. Booth, V. V. Khotkevich, S. V. Morozov, and A. K. Geim, Two-dimensional atomic crystals, Proc. Natl. Acad. Sci. USA **102**, 10451 (2005).

[3] D. C. Elias, R. V. Gorbachev, A. S. Mayorov, S. V. Morozov, A. A. Zhukov, P. Blake, L. A. Ponomarenko, I. V. Grigorieva, K. S. Novoselov, F. Guinea, and A. K. Geim, Dirac cones reshaped by interaction effects in suspended graphene, Nat. Phys. **7**, 701 (2011).

[4] K. F. Mak, C. Lee, J. Hone, J. Shan, and T. F. Heinz, Atomically Thin MoS_2: A New Direct-Gap Semiconductor, Phys. Rev. Lett. **105**, 136805 (2010).

[5] A. Castellanos-Gomez, M. Poot, G. A. Steele, H. S. J. van der Zant, N. Agraït, and G. Rubio-Bollinger, Elastic properties of freely suspended MoS_2 nanosheets, Adv. Mater. **24**, 772 (2012).

[6] Y. Y. Hui, X. Liu, W. Jie, N. Y. Chan, J. Hao, Y.-T. Hsu, L.-J. Li, W. Guo, and S. P. Lau, Exceptional tunability of band energy in a compressively strained trilayer MoS_2 sheet, ACS Nano **7**, 7126 (2013).

[7] L. Dell'Anna, Y. He, and M. Merano, Reflection, transmission, and surface susceptibility tensor of two-dimensional materials, Phys. Rev. A **105**, 053515 (2022).

[8] Z. Xu, D. Ferraro, A. Zaltron, N. Galvanetto, A. Martucci, L. Sun, P. Yang, Y. Zhang, Y. Wang, Z. Liu, J. D. Elliott, M. Marsili, L. Dell'Anna, P. Umari, and M. Merano, Optical detection of the susceptibility tensor in two-dimensional crystals, Commun. Phys. **4**, 215 (2021).

[9] E. M. Lifshitz, The theory of molecular attractive forces between solids, Sov. Phys. JETP **2**, 73 (1956).

[10] H. B. G. Casimir and D. Polder, The influence of retardation on the London–van der Waals forces, Phys. Rev. **73**, 360 (1948).

[11] J. D. van der Waals, On the continuity of the gaseous and liquid state, Ph.D. thesis, University of Leiden, (1873).

[12] J. Yang, Z. Liu, F. Grey, Z. Xu, X. Li, Y. Liu, M. Urbakh, Y. Cheng, and Q. Zheng, Observation of High-Speed Microscale Superlubricity in Graphite, Phys. Rev. Lett. **110**, 255504 (2013).

[13] Z. Zhang, J. Yin, X. Liu, J. Li, J. Zhang, and W. Guo, Substrate-sensitive graphene oxidation, J. Phys. Chem. Lett. **7**, 867 (2016).

[14] B. Li, J. Yin, X. Liu, H. Wu, J. Li, X. Li, and W. Guo, Probing van der Waals interactions at two-dimensional heterointerfaces, Nat. Nanotechnol. **14**, 567 (2019).

[15] X. Liu, J. Yang, and W. Guo, Semiempirical van der Waals method for two-dimensional materials with incorporated dielectric functions, Phys. Rev. B **101**, 045428 (2020).

[16] H. Rokni and W. Lu, Direct measurements of interfacial adhesion in 2D materials and van der Waals heterostructures in ambient air, Nat. Commun. **11**, 5607 (2020).

[17] N. Kavokine, M.-L. Bocquet, and L. Bocquet, Fluctuation-induced quantum friction in nanoscale water flows, Nature (London) **602**, 84 (2022).

[18] P. Hohenberg and W. Kohn, Inhomogeneous electron gas, Phys. Rev. **136**, B864 (1964).

[19] W. Kohn and L. J. Sham, Self-consistent equations including exchange and correlation effects, Phys. Rev. **140**, A1133 (1965).

[20] J. Harl and G. Kresse, Cohesive energy curves for noble gas solids calculated by adiabatic connection fluctuation-dissipation theory, Phys. Rev. B **77**, 045136 (2008).

[21] B. Li, X. Liu, and W. Guo, Probing interactions at two-dimensional heterointerfaces by boron nitride-wrapped tip, Nano Res. **14**, 692 (2021).

[22] Y. Chen, Y. Zhang, T. Chang, and Z. Guo, Theoretical study of entropy-induced friction in graphene, Thin-Walled Struct. **186**, 110724 (2023).

[23] M. Liao, P. Nicolini, L. Du, J. Yuan, S. Wang, H. Yu, J. Tang, P. Cheng, K. Watanabe, T. Taniguchi, L. Gu, V. E. P. Claerbout, A. Silva, D. Kramer, T. Polcar, R. Yang, D. Shi, and G. Zhang, Ultra-low friction and edge-pinning effect in large-lattice-mismatch van der Waals heterostructures, Nat. Mater. **21**, 47 (2022).

[24] X. Ding, G. Ding, X. Xie, F. Huang, and M. Jiang, Direct growth of few layer graphene on hexagonal boron nitride by chemical vapor deposition, Carbon **49**, 2522 (2011).

[25] G.-H. Lee, R. C. Cooper, S. J. An, S. Lee, A. van der Zande, N. Petrone, A. G. Hammerberg, C. Lee, B. Crawford, W. Oliver, J. W. Kysar, and J. Hone, High-strength chemical-vapor-deposited graphene and grain boundaries, Science **340**, 1073 (2013).

[26] Y.-W. Son, M. L. Cohen, and S. G. Louie, Half-metallic graphene nanoribbons, Nature (London) **444**, 347 (2006).

[27] Z. Zhang, C. Chen, and W. Guo, Magnetoelectric Effect in Graphene Nanoribbons on Substrates via Electric Bias Control of Exchange Splitting, Phys. Rev. Lett. **103**, 187204 (2009).

[28] A. Y. Nikitin, F. Guinea, F. J. García-Vidal, and L. Martín-Moreno, Edge and waveguide terahertz surface plasmon modes in graphene microribbons, Phys. Rev. B **84**, 161407 (2011).

[29] L. Ju, B. Geng, J. Horng, C. Girit, M. Martin, Z. Hao, H. A. Bechtel, X. Liang, A. Zettl, Y. R. Shen, and F. Wang, Graphene plasmonics for tunable terahertz metamaterials, Nat. Nanotechnol. **6**, 630 (2011).

[30] B. Huang, M. Liu, N. Su, J. Wu, W. Duan, B.-l. Gu, and F. Liu, Quantum Manifestations of Graphene Edge Stress and Edge Instability: A First-Principles Study, Phys. Rev. Lett. **102**, 166404 (2009).

[31] Ç. Ö. Girit, J. C. Meyer, R. Erni, M. D. Rossell, C. Kisielowski, L. Yang, C.-H. Park, M. F. Crommie, M. L. Cohen, S. G. Louie, and A. Zettl, Graphene at the edge: Stability and dynamics, Science **323**, 1705 (2009).

[32] S. Grimme, J. Antony, S. Ehrlich, and H. Krieg, A consistent and accurate *ab initio* parametrization of density functional dispersion correction (DFT-D) for the 94 elements H-Pu, J. Chem. Phys. **132**, 154104 (2010).

[33] A. Tkatchenko, R. A. DiStasio, R. Car, and M. Scheffler, Accurate and Efficient Method for Many-Body van der Waals Interactions, Phys. Rev. Lett. **108**, 236402 (2012).

[34] T. Björkman, A. Gulans, A. V. Krasheninnikov, and R. M. Nieminen, Van der Waals Bonding in Layered Compounds from Advanced Density-Functional First-Principles Calculations, Phys. Rev. Lett. **108**, 235502 (2012).

[35] N. Marom, J. Bernstein, J. Garel, A. Tkatchenko, E. Joselevich, L. Kronik, and O. Hod, Stacking and Registry Effects in Layered Materials: The Case of Hexagonal Boron Nitride, Phys. Rev. Lett. **105**, 046801 (2010).

[36] A. Tkatchenko and M. Scheffler, Accurate Molecular van der Waals Interactions from Ground-State Electron Density and Free-Atom Reference Data, Phys. Rev. Lett. **102**, 073005 (2009).

[37] J. F. Dobson, K. McLennan, A. Rubio, J. Wang, T. Gould, H. M. Le, and B. P. Dinte, Prediction of dispersion forces: Is there a problem? Aust. J. Chem. **54**, 513 (2002).

[38] F. Intravaia and A. Lambrecht, Surface Plasmon Modes and the Casimir Energy, Phys. Rev. Lett. **94**, 110404 (2005).

[39] J. F. Dobson, A. White, and A. Rubio, Asymptotics of the Dispersion Interaction: Analytic Benchmarks for van der Waals Energy Functionals, Phys. Rev. Lett. **96**, 073201 (2006).

[40] M. Tas and B. Tanatar, Plasmonic contribution to the van der Waals energy in strongly interacting bilayers, Phys. Rev. B **81**, 115326 (2010).

[41] A. L. Fetter, Edge magnetoplasmons in a bounded two-dimensional electron fluid, Phys. Rev. B **32**, 7676 (1985).

[42] X. Xia and J. J. Quinn, Multipole edge plasmons of two-dimensional electron-gas systems, Phys. Rev. B **50**, 8032 (1994).

[43] W. Wang, P. Apell, and J. Kinaret, Edge plasmons in graphene nanostructures, Phys. Rev. B **84**, 085423 (2011).

[44] Z. Zhang, Y. Yang, G. Gao, and B. I. Yakobson, Two-dimensional boron monolayers mediated by metal substrates, Angew. Chem., Int. Ed. **54**, 13022 (2015).

[45] B. Feng, J. Zhang, Q. Zhong, W. Li, S. Li, H. Li, P. Cheng, S. Meng, L. Chen, and K. Wu, Experimental realization of two-dimensional boron sheets, Nat. Chem. **8**, 563 (2016).

[46] C.-C. Liu, W. Feng, and Y. Yao, Quantum Spin Hall Effect in Silicene and Two-Dimensional Germanium, Phys. Rev. Lett. **107**, 076802 (2011).

[47] A. Fleurence, R. Friedlein, T. Ozaki, H. Kawai, Y. Wang, and Y. Yamada-Takamura, Experimental Evidence for Epitaxial Silicene on Diboride Thin Films, Phys. Rev. Lett. **108**, 245501 (2012).

[48] V. A. Parsegian, *Van der Waals Forces: A Handbook for Biologists, Chemists, Engineers, and Physicists* (Cambridge University Press, Cambridge, 2005).

[49] *Casimir Physics*, Lecture Notes in Physics Vol. 834, edited by D. Dalvit, P. Milonni, D. Roberts, and F. Da Rosa (Springer, Berlin, 2011).

[50] N. W. Ashcroft and N. D. Mermin, *Solid State Physics* (Holt, Rinehart and Winston, New York, 1976).

[51] Y. Huang, S. N. Shirodkar, and B. I. Yakobson, Two-dimensional boron polymorphs for visible range plasmonics: A first-principles exploration, J. Am. Chem. Soc. **139**, 17181 (2017).

[52] G. W. Hanson, Quasi-transverse electromagnetic modes supported by a graphene parallel-plate waveguide, J. Appl. Phys. **104**, 084314 (2008).

[53] A. Scholz, T. Stauber, and J. Schliemann, Plasmons and screening in a monolayer of MoS_2, Phys. Rev. B **88**, 035135 (2013).

[54] M. S. Ukhtary, A. R. T. Nugraha, E. H. Hasdeo, and R. Saito, Broadband transverse electric surface wave in silicene, Appl. Phys. Lett. **109**, 063103 (2016).

[55] B. Hu, Screening-induced carrier transport in silicene, J. Phys.: Condens. Matter **27**, 245301 (2015).

[56] M. Abramowitz and I. A. Stegun, *Handbook of Mathematical Functions with Formulas, Graphs and Mathematical Tables*, National Bureau of Standards Applied Mathematics Series No. 55 (National Bureau of Standards, Washington, DC, 1965).

[57] X. Chu and A. Dalgarno, Linear response time-dependent density functional theory for van der Waals coefficients, J. Chem. Phys. **121**, 4083 (2004).

[58] V. Blum, R. Gehrke, F. Hanke, P. Havu, V. Havu, X. Ren, K. Reuter, and M. Scheffler, *Ab initio* molecular simulations with numeric atom-centered orbitals, Comput. Phys. Commun. **180**, 2175 (2009).

[59] J. P. Perdew, K. Burke, and M. Ernzerhof, Generalized Gradient Approximation Made Simple, Phys. Rev. Lett. **77**, 3865 (1996).

[60] W. Gao and A. Tkatchenko, Sliding Mechanisms in Multilayered Hexagonal Boron Nitride and Graphene: The Effects of Directionality, Thickness, and Sliding Constraints, Phys. Rev. Lett. **114**, 096101 (2015).

[61] S. Tsoi, P. Dev, A. L. Friedman, R. Stine, J. T. Robinson, T. L. Reinecke, and P. E. Sheehan, Van der Waals screening by single-layer graphene and molybdenum disulfide, ACS Nano **8**, 12410 (2014).

[62] X. Liu, Z. Zhang, and W. Guo, Van der Waals screening by graphenelike monolayers, Phys. Rev. B **97**, 241411 (2018).

[63] A. Ambrosetti and P. L. Silvestrelli, Hidden by graphene—towards effective screening of interface van der Waals interactions via monolayer coating, Carbon **139**, 486 (2018).

[64] M. Li, J. R. Reimers, J. F. Dobson, and T. Gould, Faraday cage screening reveals intrinsic aspects of the van der Waals attraction, Proc. Natl. Acad. Sci. USA **115**, E10295 (2018).

[65] C. R. Dean, A. F. Young, I. Meric, C. Lee, L. Wang, S. Sorgenfrei, K. Watanabe, T. Taniguchi, P. Kim, K. L. Shepard, and J. Hone, Boron nitride substrates for high-quality graphene electronics, Nat. Nanotechnol. **5**, 722 (2010).

[66] M. Yankowitz, J. Xue, D. Cormode, J. D. Sanchez-Yamagishi, K. Watanabe, T. Taniguchi, P. Jarillo-Herrero, P. Jacquod, and B. J. LeRoy, Emergence of superlattice Dirac points in graphene on hexagonal boron nitride, Nat. Phys. **8**, 382 (2012).

[67] C. Lin, B. Wang, K. H. Teo, and Z. Zhang, Near-field enhancement of thermoradiative devices, J. Appl. Phys. **122**, 143102 (2017).